Nanoscale

ROYAL SOCIETY OF CHEMISTRY

PAPER

Published on 08 July 2024
Licence and permissions

Check for updates

Cite this: *Nanoscale*, 2024, **16**, 13915

Efficient detection of *p*-nitrophenol *via* a polypyrrole flower-decorated nickel foam-based electrochemical sensor†

Shiv Dutta Lawaniya,[a] Gaurav Pandey,[a] Yeontae Yu[b] and Kamlendra Awasthi *[a]

p-Nitrophenol (*p*-NP) is known as a common contaminant found in wastewater, agricultural runoff, and industrial effluents which can degrade water quality and cause potential carcinogenic and toxic effects on the human body. Its detection is essential for public health, industrial safety, environmental protection, and regulatory compliance, underscoring its broad applicability. In this study, a novel electrochemical sensor based on polypyrrole (PPy) flowers assembled *via* nanotubes was developed for the sensitive determination of *p*-NP. The nickel (Ni) foam modified with PPy flowers functioned as the working electrode and showed selectivity toward *p*-NP in a phosphate buffer medium at pH 7.0. Cyclic voltammetry (CV) and differential pulse voltammetry (DPV) techniques were utilized for the sensitive determination of *p*-NP. Under the optimum conditions, the peak currents of DPV *versus* the concentrations of *p*-NP in the range of 0.01–20 nM showed a good linear relationship (R^2 = 0.9943), and the limit of detection (LOD) was calculated to be 7.18 pM (signal-to-noise ratio of 3, S/N = 3). The fabricated electrochemical *p*-NP sensor exhibited high sensitivity, a low detection limit, and a low response time. The recoveries of *p*-NP in real samples of groundwater and tap water using the PPy Fls/Ni foam electrode were in the range of 91.0–108.4% with a relative standard deviation (RSD) in the range of 6.65%. Consequently, the PPy Fls/Ni foam electrode could be applied as a rapid, precise, and sensitive electrochemical sensor platform for aqueous *p*-NP quantification and determination.

Received 11th April 2024,
Accepted 20th June 2024

DOI: 10.1039/d4nr01580k

rsc.li/nanoscale

1. Introduction

The release of organic contaminants into the atmosphere and water supplies during the past few decades has posed a serious threat to the ecosystem. Substituted phenol compounds, which are highly poisonous and resistant to microbes, are important byproducts and raw materials of many chemical companies.[1,2] The production of herbicides, insecticides, disinfectants, and colors frequently involves phenolic compounds with one or more aromatic rings and hydroxyl groups.[3] *p*-Nitrophenol, a type of substituted phenol, is listed as a priority pollutant by the US Environmental Protection Agency (EPA) because of its detrimental effects on human, animal, plant growth and metabolism.[4,5] Thousands of tons of industrial waste are released into the environment as a result of extensive industrial activities, endangering soils, groundwater, and subsurface water.[6] It is therefore quite likely to enter the bodies of humans and other animals through the food chain.[7–10] Humans may experience a variety of physiological symptoms after acutely ingesting or inhaling *p*-NP, including cyanosis, nausea, sleepiness, and headaches.[11] Accurately identifying the *p*-NP concentration at which it is ecologically innocuous is essential. Consequently, there is an urgent need for an accurate, affordable, quick, and trustworthy analytical instrument for the high-sensitivity detection and quantification of *p*-NP.

Over the past few decades, several laboratory-based analytical techniques have been developed for detecting *p*-NP, including gas and liquid chromatography, UV-vis spectrophotometry, spectrofluorimetry, and their combinations.[12,13] These methods often require skilled operators and costly, complicated and challenging equipment that cannot be utilized on-site.[14] Electrochemical sensing approaches have gained popularity for determining *p*-NP due to their advantages, including ease of use, rapidity, selectivity, inexpensive nature, miniaturization, and online monitoring.[15] Furthermore, electrochemically removing nitro groups in aromatic or heterocyclic compounds allows for the sensitive determination of *p*-NP using electrode materials. Sensing electrodes can be modified with

[a]*Department of Physics, Malaviya National Institute of Technology Jaipur, Jaipur-302017, Rajasthan, India. E-mail: kawasthi.phy@mnit.ac.in*
[b]*Division of Advanced Materials Engineering, Jeonbuk National University, 567, Baekje daero, Deokjin-gu, Jeonju, 54896, South Korea*

†Electronic supplementary information (ESI) available. See DOI: https://doi.org/10.1039/d4nr01580k

various materials, including organic, inorganic, metallic, polymeric, and biological molecules, to enhance sensitivity and selectivity.[16]

In recent years, the integration of conductive polymers has demonstrated great enhancement in the electrochemical efficiency of electrodes.[17,18] In particular, polypyrrole (PPy) has drawn a lot of interest because of its superior environmental stability, high surface area, large energy storage capacity, and outstanding electrical conductivity.[19–21] PPy produced by chemical or electrochemical polymerization techniques has been used extensively in electrochemical sensing applications up to this point.[22–24] However, much research has not been done on using PPy nanostructures for the electrochemical detection of *p*-NP. The various nanostructures of PPy, such as nanorods, nanotubes, flowers, urchins, spheres, *etc*., exhibit a very high surface area, which provides a large number of active sites for target molecules. An electrochemical sensor for *p*-NP was reported by Arulraj *et al.*[25] using an electrochemically treated nano-polypyrrole/sodium dodecyl sulfate screen (ENPPy/SDS film) modified glassy carbon electrode. The suggested sensor shows a broad linear range from 0.1 nM to 100 μM and a very low detection limit of 0.1 nM. In another work, Tighilt *et al.*[26] developed polypyrrole deposited on a porous oxidized silicon substrate using an electrochemical method for the detection of *p*-NP. The sensor linearity is observed within the concentration range of 10^{-2} to 10^{-8} M, suggesting a satisfactory calibration. Similarly, Faisal *et al.*[27] developed a selective *p*-NP sensor on a glassy carbon electrode (GCE), which was decorated with sol–gel-prepared Pt nanoparticle (NP) embedded polypyrrole-carbon black (PPy-CB)/ZnO nanocomposites (NCs).

In this work, we have developed a *p*-nitrophenol (*p*-NP) electrochemical sensor based on a PPy flower modified nickel foam (NF) electrode. Polypyrrole flowers were synthesized *via* a template-assisted method by using MnO_2 nanostructures as templates. The electrochemical sensor was characterized using cyclic voltammetry (CV) and differential pulse voltammetry (DPV) techniques. PPy flowers have considerable potential in the detection of nitrophenols, as demonstrated by their electrochemical catalytic behavior and sensing performance to *p*-NP.

2. Materials and methods

Reagents and materials

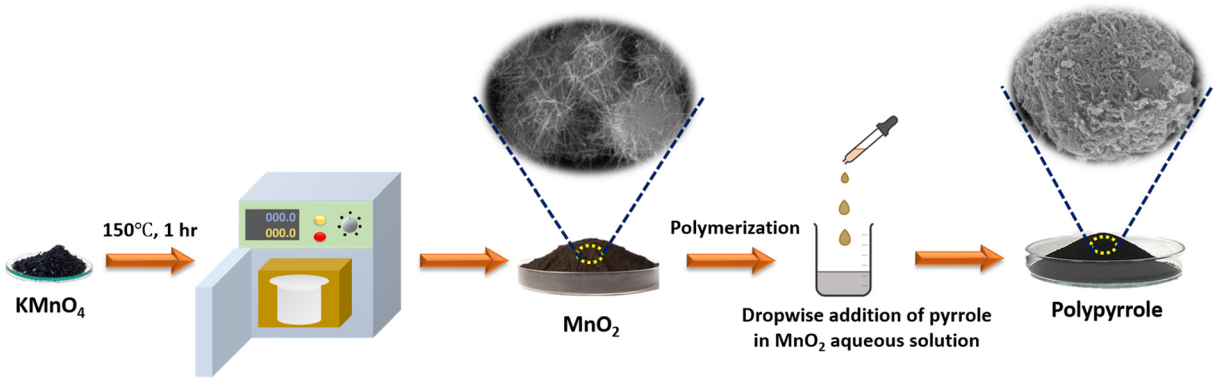
Pyrrole (98%, Sigma Aldrich), *p*-nitrophenol (99%, Sigma Aldrich), $KMnO_4$ (98.5%, Merck), and $FeCl_3$ (98%, CDH) were employed in the synthesis procedure. Hydrochloric acid (HCl) and nitric acid (HNO_3) were purchased from Merck. For electrode preparation, nickel (Ni) foam (Kanopy Techno, 99%) and *N*-methyl pyrrolidone (Alfa Aesar, C_5H_9NO, 99+%) were used as a substrate and solvent, respectively. All analytical-grade compounds were used exactly as supplied, requiring no additional purification.

Synthesis of polypyrrole (PPy) flowers

Manganese dioxide (MnO_2) flowers were synthesized using the hydrothermal method and utilized as templates to synthesize PPy flower nanostructures. The synthesis procedure of MnO_2 nanostructures and PPy flowers from MnO_2 templates is reported in our previous literature.[28] Typically, using ultrasonication, 100 mg of MnO_2 templates were dispersed in 20 ml of 0.1 M HCl solution. 71 μl of pyrrole was added to the previously prepared solution and vigorously stirred after suitable dispersion. The reaction proceeded quickly, and the brownish MnO_2 suspension immediately turned black. The suspension was allowed for an hour to continue polymerization statically after 15 minutes of vigorous stirring. The end product was dried at 60 °C after being meticulously cleaned with ethanol and DI water several times. A schematic of the PPy flower synthesis is shown in Scheme 1.

Fabrication of the PPy Fls/Ni foam electrode

A bare nickel (Ni) foam having 1 cm^2 geometrical surface area was first sequentially washed and sonicated with deionized water (DI), ethanol, and acetone. For the preparation of the working electrode, a viscous slurry of the as-synthesized electrode material was prepared by grinding 10 mg of the material in a mortar and pestle with a few drops of the binder α-terpineol. Next, the thick slurry was dispersed into 10 ml of *N*-methyl pyrrolidone solvent *via* ultrasonication. Lastly, the Ni foam surface was coated with an appropriate amount of the



Scheme 1 Schematic illustration of polypyrrole flower synthesis *via* the template-assisted method.

This journal is © The Royal Society of Chemistry 2024

suspension and was then allowed to dry at 60 °C to fabricate the PPy Fls/Ni foam modified electrode.

Characterization

The surface structure of the synthesized materials was investigated using field emission scanning electron microscopy (Nova Nano 450 FEI). The Raman and FT-IR spectra were acquired using a Renishaw Raman spectrometer and a PerkinElmer Fourier transform infrared spectrophotometer, respectively. The crystallographic information of the synthesized material was obtained with an X-ray diffractometer (Panalytical XPert Pro) using a Cu Kα1 (k = 1.5406 Å) radiation source.

Electrochemical measurements

Electrochemical data were collected using a Squidstat Plus electrochemical workstation (USA) using a traditional three-electrode configuration consisting of a platinum wire auxiliary electrode, an Ag/AgCl reference electrode, and a working electrode in 0.01 M phosphate-buffered saline (PBS). Cyclic voltammograms (CV) were recorded *versus* saturated Ag/AgCl between −1.0 and 0.2 V at a scan rate of 50 mV s^{-1}. Differential pulse voltammetry (DPV) was conducted at an initial potential of −1.0 V and a final potential of 0.2 V, with the pulse height, width, and period as 0.02 V, 0.1 s, and 0.2 s, respectively. For the detection of *p*-NP, a stock solution of 1 μM *p*-NP was prepared and further diluted to different concentrations.

3. Results and discussion

3.1 Characterization of polypyrrole (PPy) flowers

The structural and elemental analysis of PPy flowers synthesized using the template-assisted approach was carried out using FESEM with EDS as shown in Fig. 1. Fig. 1(a & b) depicts the surface topography of the nanotube-assembled flower-like structure, which shows hierarchical 3D flower-like microspheres with a diameter of about 0.52 μm. The SEM images of the MnO_2 flower-like nanostructures are displayed in Fig. S1.† Pyrrole monomers are evenly coated on the outer surface of MnO_2 during the polymerization process, where they subsequently expand into oligomers to produce the polymer.[29,30] Concurrently, MnO_2 templates are eliminated through the

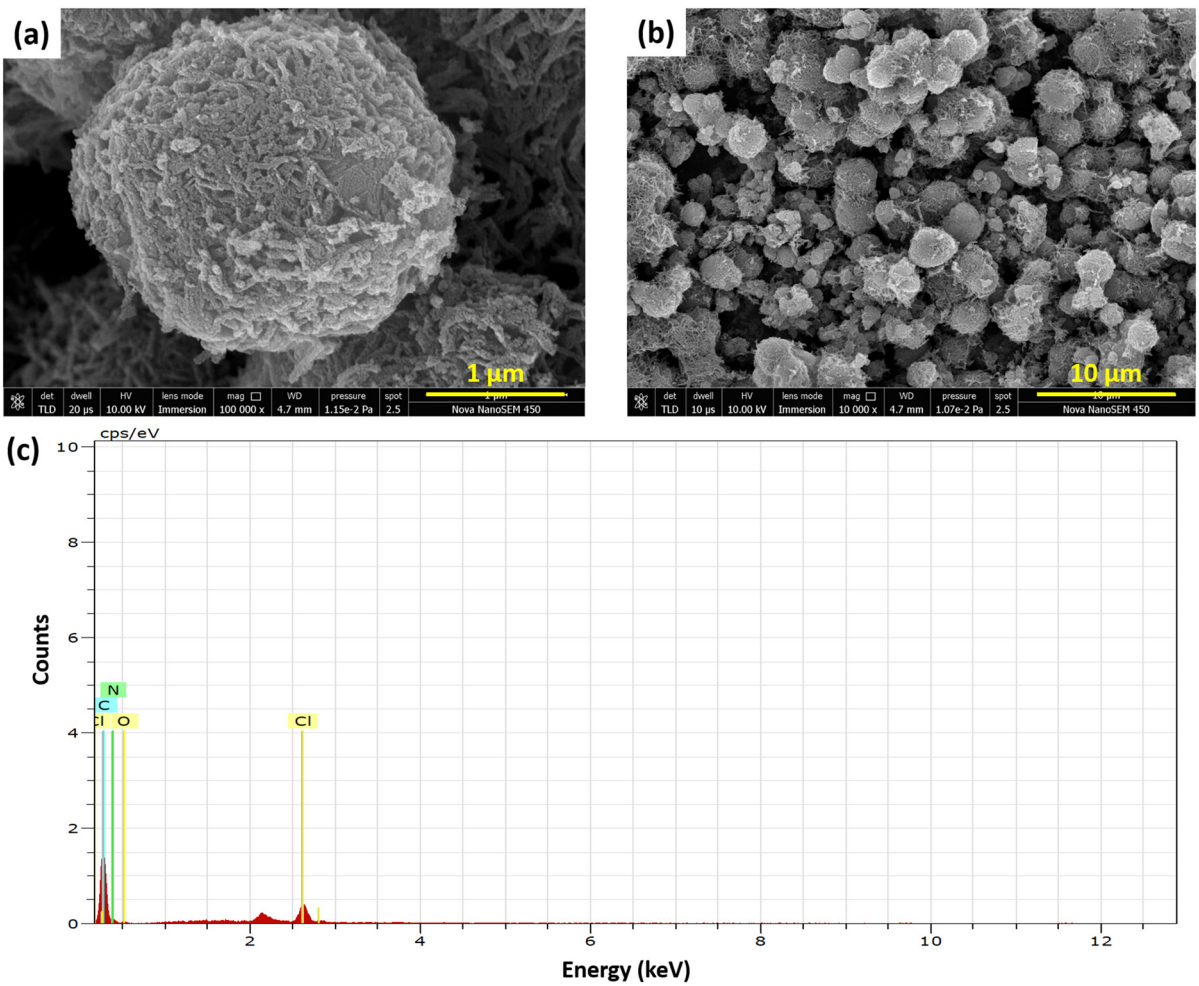


Fig. 1 SEM images of polypyrrole (PPy) flowers (a & b) and EDS spectra of PPy flowers (c).

reduction of MnO_2 into Mn^{2+} ions. Compared to MnO_2 nanostructures, polypyrrole nanostructures were found to have larger dimensions, which indicates polypyrrole's outward expansion through a diffusion-controlled mechanism.[31–33]

Furthermore, the elemental composition of the as-synthesized PPy was analyzed by energy-dispersive spectroscopy (EDS), as shown in Fig. 1c. The spectra indicate the intrinsic elements of PPy, *i.e.* nitrogen, carbon, and adsorbed oxygen along with no additional peak of Mn showing complete removal of the MnO_2 template. The presence of a small amount of Cl in PPy illustrates the doping of Cl in the PPy structure, which enhances its conductivity.

Raman spectroscopy was employed to further analyse the structural properties of PPy flowers. The Raman spectrum of PPy flowers is shown in Fig. 2a. The ring stretching mode and C=C backbone stretching vibrations in PPy are represented by the intense bands that are seen around 1348 cm^{-1} and 1560 cm^{-1}, respectively.[34–37] The peak around 1348 cm^{-1} is related to the C–N bond stretching present in the chemical structure of polypyrrole. This bond is a type of covalent bond that forms between the pyrrole ring carbon atom and nitrogen, and has a typical bond length of 1.33 Å.[38] The conjugated π-electron system of PPy is facilitated by the single pair of electrons that the N atom in the pyrrole ring possesses.[39] The conductivity of polypyrrole depends on this electron delocalization.[40] Furthermore, the second peak is associated with the C=C backbone stretching in the polypyrrole structure. The symmetric or asymmetric stretching vibration of the carbon–carbon double bonds in the polypyrrole backbone is referred to as the C=C stretching mode.[41] The C=C bonds are a component of a conjugated system in which the π-electrons are dispersed throughout the polymer backbone.[42,43]

These findings demonstrate the effective synthesis of polypyrrole using a template-assisted method. Fig. 2b shows the FT-IR spectrum of PPy where O–H and N–H symmetric stretching vibrations are responsible for the peaks that were detected at 3560 and 3434 cm^{-1}.[44] The C=C ring stretching vibrations are represented by the characteristic peaks at 1623 and 1548 cm^{-1}.[45,46] The vibrations of C=N bending, C–N stretching, and C–H bending are associated with the peaks at 1300, 1192, and 1043 cm^{-1}, respectively.[47] Additionally, the C–H out-of-plane deformation vibration mode is responsible for the peaks at 924 and 660 cm^{-1}.[48] Furthermore, the X-ray diffraction spectrum of pure PPy is shown in Fig. 2c. The PPy XRD pattern has a large peak around 24°, indicating that the material is amorphous in nature.[49,50] The interplanar spacing of the PPy chains is responsible for the structural ordering observed at the nanoscale. This is common for low-degree crystallinity nanostructured polymers.[51]

3.2 Electrochemical characterization

3.2.1 Electrochemical behaviour of the PPy Fls/Ni foam toward *p*-nitrophenol (*p*-NP). The cyclic voltammetry (CV) method was employed to examine the electrocatalytic performance of this PPy Fls/Ni foam toward *p*-NP using a three-electrode system in 0.1 M PBS (pH 7) electrolyte solution. For comparison, bare Ni foam was also evaluated. The cyclic voltammograms (CVs) of PPy Fls/Ni foam and bare Ni foam in 0.1 M PBS with and without 10 nM *p*-NP at a scan rate of 50 mV s^{-1} within the potential range of −1.0 to 0.2 V are shown in Fig. 3a.

The response current observed on the PPy Fls/Ni foam electrode with 10 nM *p*-NP is 0.4 mAmp, which is significantly higher than the measured current on the bare nickel foam electrode (0.09 mAmp). The results reveal that the PPy Fls/Ni foam electrode has excellent electroactivity towards *p*-NP. In the presence of *p*-NP, the PPy Fls/Ni foam electrode has a larger closed area than the bare nickel foam, demonstrating that the bare nickel foam has no noticeable electrochemical response. Furthermore, in the presence of *p*-NP, the PPy Fls/Ni foam electrode demonstrates a higher response current (0.4 mAmp) of the anodic peak than in the absence of *p*-NP (0.27 mAmp). The findings also endorse the PPy Fls/Ni foam electrode's strong electrochemical sensing capabilities for *p*-NP. The high surface area, excellent electrical conductivity, and synergistic effect of PPy flowers and nickel foam contribute to the enhanced current response.

The PPy Fls/Ni foam electrode exhibited distinct peaks for reduction and oxidation at −0.74 V and −0.25 V, respectively. Previous findings state that at −0.74 V on the reduction side, *p*-NP was reduced into *p*-hydroxyaminophenol with four electrons and a proton transfer.[52] On the reversal scan, *p*-hydroxyaminophenol was oxidized to peroxo-aminobenzene with a proton transfer and electron transfers at −0.25 V. In most of the previously reported literature, the oxidation peak of *p*-NP

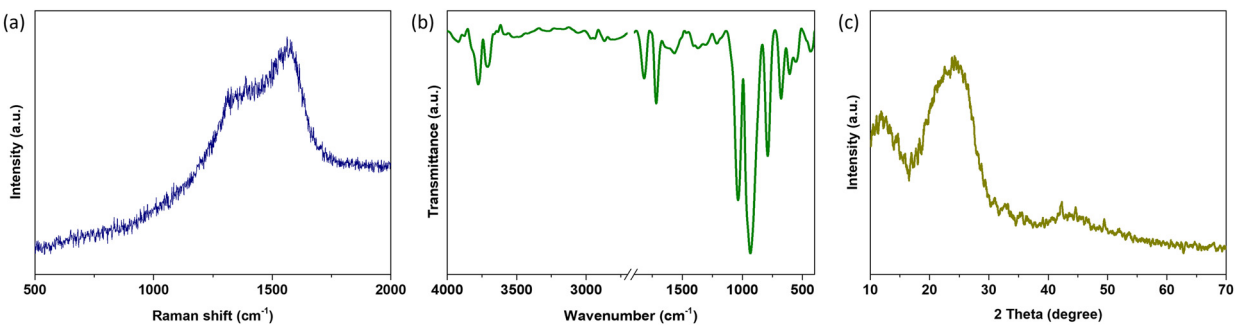


Fig. 2 Raman (a), FT-IR (b), and XRD (c) spectra of PPy flowers.

This journal is © The Royal Society of Chemistry 2024

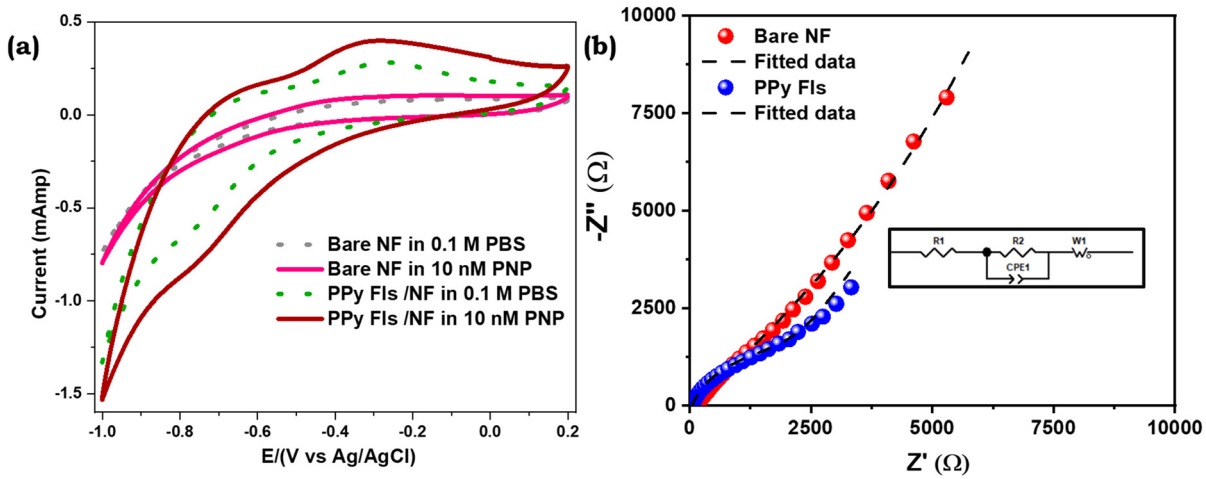


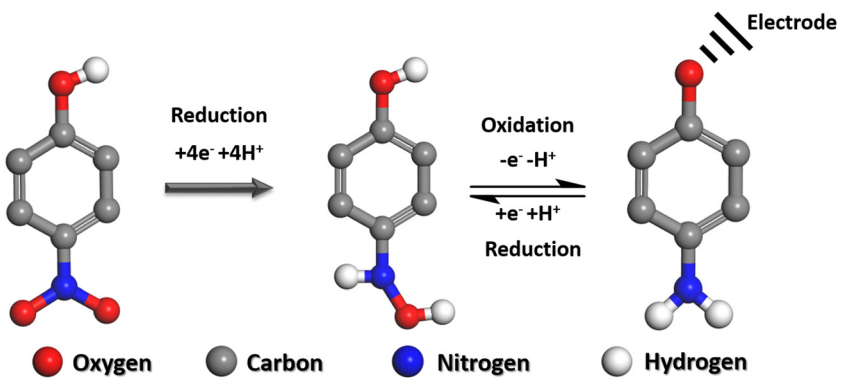
Fig. 3 (a) CV curves of bare Ni foam and PPy FIs/Ni foam electrodes with or without 10 nM *p*-NP (scan rate of 50 mV s^{-1} in 0.1 M PBS electrolyte). (b) EIS of bare Ni foam and PPy FIs/Ni foam electrodes.

was observed at a positive potential around +0.15 V. However, in our case, the oxidation peak was observed around −0.25 V, which is due to the weak oxidation of reduced *p*-NP. At −0.74 V, generally irreversible reduction takes place, converting *p*-NP into an aminophenol derivative. On the oxidation side, a reversible redox reaction occurs, but in this case, the reduction peak turns out to be negligible, while oxidation peaks dominate the redox reaction.[53,54] The reaction is shown in Scheme 2.

3.2.2. EIS of the bare Ni foam and PPy FIs/Ni foam electrodes. The charge transfer resistance (R_{ct}) values of bare Ni foam and PPy FIs/Ni foam were measured using electrochemical impedance spectroscopy (EIS), as shown in Fig. 3b. The R_{ct} values were determined in 0.1 M PBS solution electrolyte medium. The R_{ct} values for bare Ni foam and PPy FIs/Ni foam were determined to be 6555 and 1674 Ω, respectively. R_{ct} with lower values represents a more inventive strategy for electron transfer kinetics, resulting in higher electrocatalytic activity. The rationale could be due to the high surface area of PPy FIs, which leads to structural potential and improved active sites.

3.2.3. Scan rate study of the PPy FIs/Ni foam electrode. The CV curves of the PPy FIs/Ni foam electrode shown in Fig. 4a are presented at varying sweep rates between 10 and 200 mV s^{-1} in the presence of 10 nM *p*-NP to investigate the reaction kinetics. As the scan rate increases, it is evident that the anodic peak moves slightly in a positive direction while the cathodic peak shifts negatively, indicating a potential kinetic limit in the oxidation of *p*-NP. Fig. 4b shows the fitted graph between the response current and the square root of scan rates. It is evident that there is a linear relationship between the response current and the square root of the scan rate, suggesting that diffusion plays a major role in controlling *p*-NP during the reaction process. Linear sweep voltammetry (LSV) of the proposed electrode for various concentrations of *p*-NP was also performed as shown in Fig. S2.†

3.2.4 Detection of *p*-nitrophenol at the PPy FIs/Ni foam electrode. Cyclic voltammetry for various *p*-NP concentrations was performed for the initial investigation of the electrocatalytic activity of PPy FIs/Ni foam toward *p*-NP. The CV curves of the PPy FIs/Ni foam electrode at different *p*-NP concentrations (ranging from 0.01 nM to 20 nM) are displayed in



Scheme 2 Electrochemical reaction mechanism of *p*-NP on the PPy FIs/Ni foam modified electrode.

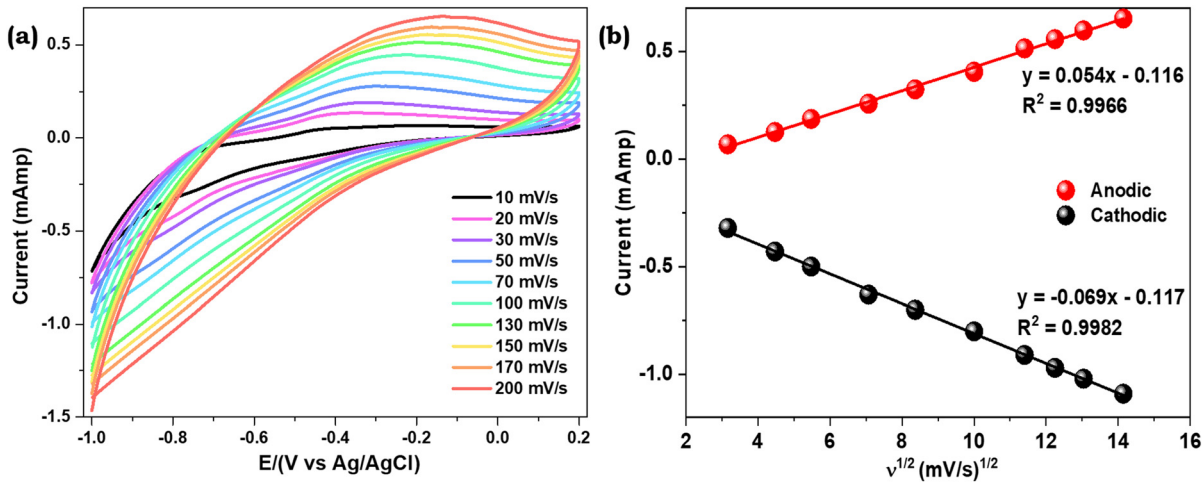


Fig. 4 (a) CV curves of the PPy Fls/Ni foam electrode scanned at 10–200 mV s^{-1} in 0.1 M PBS electrolyte after adding 10 nM *p*-NP. (b) Peak currents are related to the square root of the scan rate.

Fig. 5a. The peak currents exhibit an inclination of steady increase as the concentration of *p*-NP from lower to higher. There was a discernible increase in the oxidative peak current following the progressive addition of *p*-NP, suggesting an electrochemical interaction between polypyrrole and *p*-NP. Additionally, Fig. 5b displays the calibration plot between the anodic peak current and various *p*-NP concentrations. The results show a linear relationship between the oxidation peak and *p*-NP concentrations with linear regression I_p = 0.007C(nM) + 0.329, R^2 = 0.9949, indicating fast electron transfer and high electrocatalytic activity.

To study the analytical response of PPy towards *p*-NP, the differential pulse voltammetry (DPV) approach was utilized for the PPy Fls/Ni foam electrode at various concentrations of *p*-NP. The DPV curve response of the PPy Fls/Ni foam electrode in 0.1 M PBS with varying *p*-NP concentrations ranging between 0.01–0.1 and 0.2–20 nM is displayed in Fig. 6a. The results show that on successive addition of *p*-NP, the peak current gradually increases. Furthermore, the calibration plot between the current and *p*-NP concentrations in Fig. 6b shows a decent linear correlation (R^2 = 0.99). The linear regression equation was found to be I = 0.0053C(nM) + 0.1062. In addition, the acquired slope value was divided by the value of the electrode's active surface area to evaluate the sensitivity of the prepared electrode. Remarkably, the results showed that the PPy Fls/Ni foam electrode was highly sensitive towards *p*-NP (sensitivity: 5.37 μA nM^{-1} cm^{-2}). Furthermore, the limit of detection (LOD) of the prepared PPy Fls/Ni foam electrode towards *p*-NP was determined to be 7.18 pM based on the signal-to-noise ratio (S/N = 3).

In order to investigate the selectivity of the sensor, 2,4-dinitrophenol, chloramphenicol, ascorbic acid, glucose, and oxalic

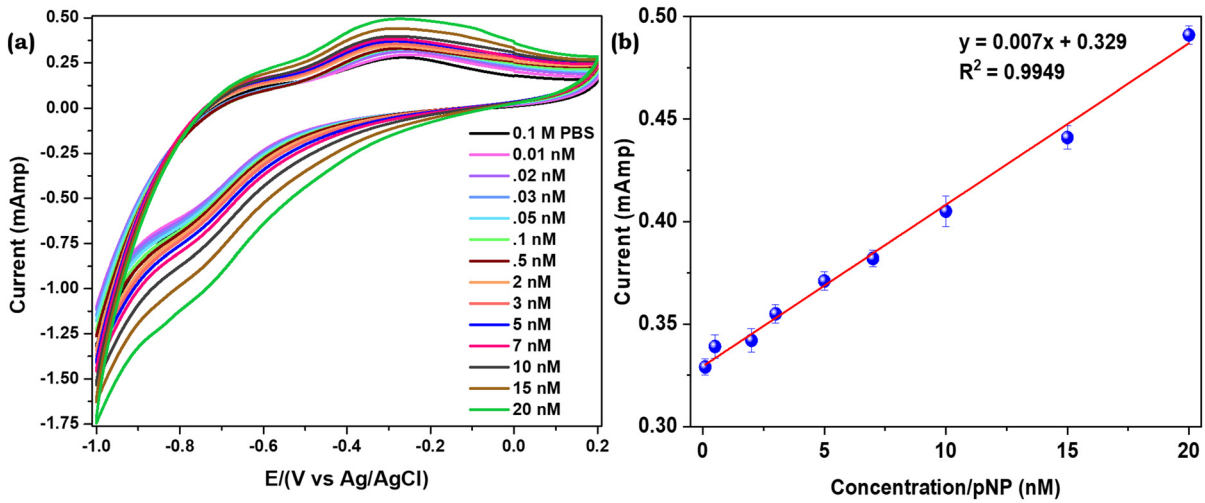


Fig. 5 (a) Cyclic voltammograms (CVs) of the PPy Fls/Ni foam electrode after the addition of different concentrations of *p*-NP from 0.01 to 20 nM. (b) Calibration plot for the concentration of *p*-NP *vs.* peak current.

This journal is © The Royal Society of Chemistry 2024

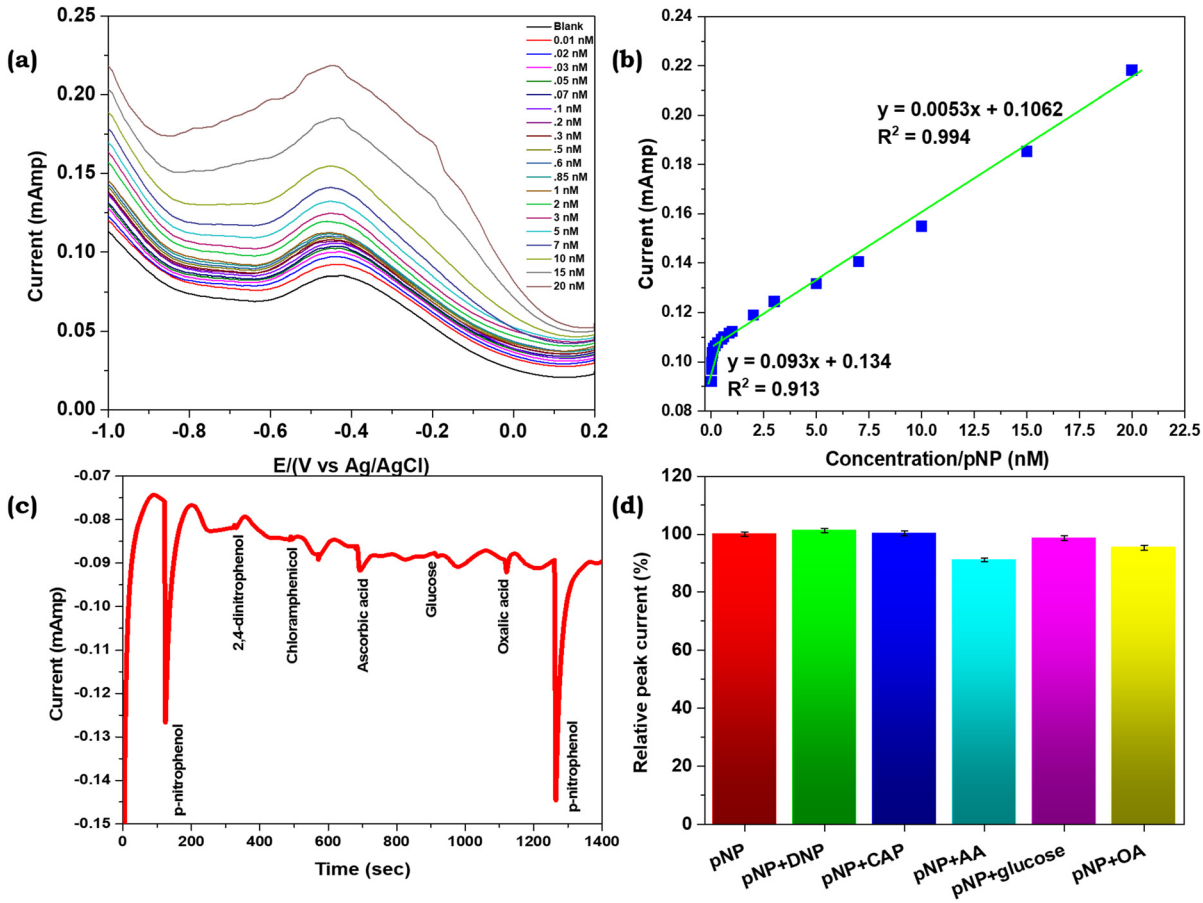


Fig. 6 (a) DPV response curves at various concentrations of *p*-NP at a scan speed of 50 mV s^{-1} in 0.1 M PBS (pH 7), (b) the corresponding calibration plot, (c) amperometric response of the PPy Fls/Ni foam sensor electrode at −0.37 V upon the addition of 10 nM *p*-NP, 2,4-dinitrophenol, chloramphenicol, ascorbic acid, glucose and oxalic acid in 0.1 M PBS electrolyte, and (d) bar graph of the relative peak current for the PPy Fls/Ni foam electrode towards sensing of *p*-NP in the presence of the various analytes.

acid were chosen as the coexisting chemicals and equivalent for the comparative tests. At an applied potential of −0.37 V, chronoamperometry was utilized to measure the current variations with respect to time. The amperometric responses of the PPy Fls/Ni foam electrode at −0.37 V in 0.1 M PBS electrolyte solution are displayed in Fig. 6c, following the addition of 10 nM *p*-NP along with other interfering agents. It is noteworthy that the modified electrode reacts to *p*-NP more strongly with a much higher current change, even in the presence of other interferents. The relative peak current (%) bar diagram of interferences is displayed in Fig. 6d. When 10 nM *p*-NP was combined with other phenolic compounds, such as 2,4-dinitrophenol and chloramphenicol, the peak current was 101% and 103% of the value obtained with *p*-NP alone. This suggests that these phenolic analytes do not significantly interfere with the detection of *p*-NP. In addition, the impact of a few biomolecule-based interfering species was also investigated. Considering that the relative peak current change is less than 10%, the interfering agents do not impact the target analyte. The large change in current upon the addition of 10 nM *p*-NP suggests good interaction between the polypyrrole chemical structure and *p*-NP. Furthermore, anti-selectivity tests have also been performed with *p*-NP's three structural analogues including 2-nitrophenol, 3-nitrophenol and 2,4-dinitrophenol at 10 nM concentration (Fig. S6†). As a result, the highest change in current was observed for *p*-NP compared to the other analytes, which shows the proposed sensor's selective nature towards *p*-NP even in a solution containing its structural analogues.

The response time of the fabricated PPy Fls/Ni foam electrode was calculated by plotting the current *vs.* time at the time of exposure to 10 nM *p*-NP (Fig. 7a). The observed response time of the sensor is 3.13 s at a *p*-NP concentration of 10 nM.

The long-term stability of the sensors is crucial for real-world applications. In this case, the PPy Fls/Ni foam electrode stability was examined by tracking its reactions to 10 nM *p*-NP for 7 days in an ambient environment, and the results are shown in Fig. 7b. Prior to testing, the electrode was kept at room temperature. The electrode response current of *p*-NP remained above 95% for seven days, suggesting that the PPy Fls/Ni foam electrode has a significant stability. This can be

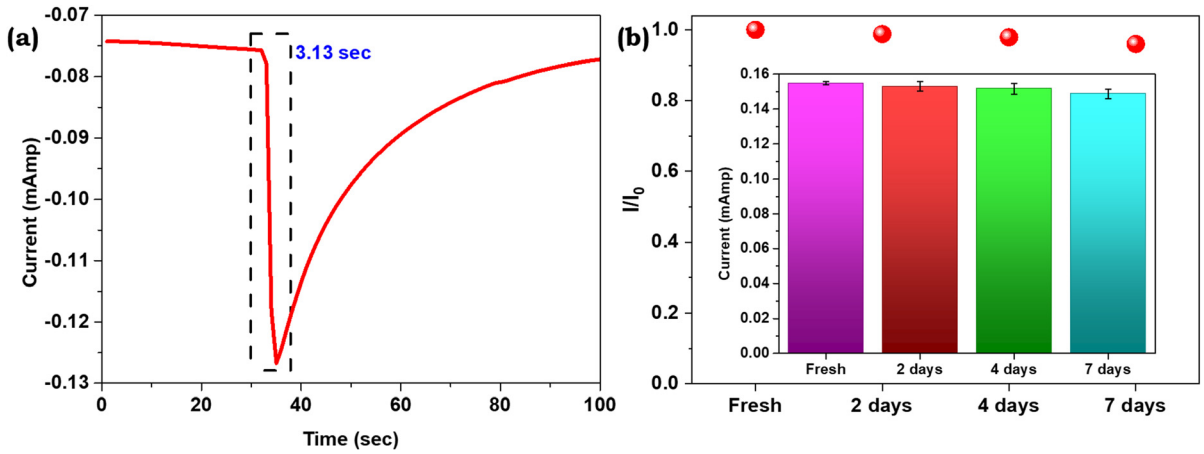


Fig. 7 (a) The response time of the PPy Fls/Ni foam electrode when 10 nM *p*-NP was added. (b) The current response in 0.1 M PBS electrolyte towards 10 nM *p*-NP on the same electrode within 7 days.

explained by the superior chemical corrosion resistance, higher wear resistance, and stable chemical characteristics of polypyrrole. The DPV of the electrochemical sensor for 7 days is presented in Fig. S3.†

Furthermore, the repeatability and reproducibility of the developed PPy Fls/Ni foam-based sensor were also evaluated (Fig. 8a and b). Using the same electrode, the repeatability was assessed ten times for *p*-NP (10 nM) detection. Fig. 8a shows that there is no considerable change in the current for successive repetitions and the relative standard deviation (RSD) was found to be 0.9% indicating good repeatability of the electrode. In order to examine the reproducibility of the sensor, three electrodes were concurrently fabricated under identical conditions. For the detection of *p*-NP (10 nM), a low RSD of 0.84% was found, demonstrating remarkable reproducibility (Fig. 8b).

Table 1 presents a comparative study of *p*-NP sensors based on several types of sensing electrode materials reported in the previous literature.

3.2.5 Applicability of the PPy Fls/Ni foam electrode in real samples. In order to assess the functionality of the modified Ni foam electrode, recovery measurements were performed to determine the content of *p*-NP in real water samples. To prepare solutions with varying concentrations, the *p*-NP solution was combined with the electrolyte solution containing ground and tap water, which were utilized as real water samples. DPV curves were acquired with varying concentrations of each sample. Table 2 displays the spiked and recovered concentration results in which the observed recoveries fell within the range of 91–108.4% for groundwater and 93.4–105% for tap water samples, respectively. The PPy Fls/Ni foam electrode demonstrated a satisfactory recovery rate for the assessment of *p*-NP in real samples, indicating that the *p*-NP detection approach presented in this work holds promise for the direct examination of environmental samples. The DPV of the PPy Fls/Ni foam electrode in real water samples at different spiked *p*-NP concentrations is shown in Fig. S4 and 5.†

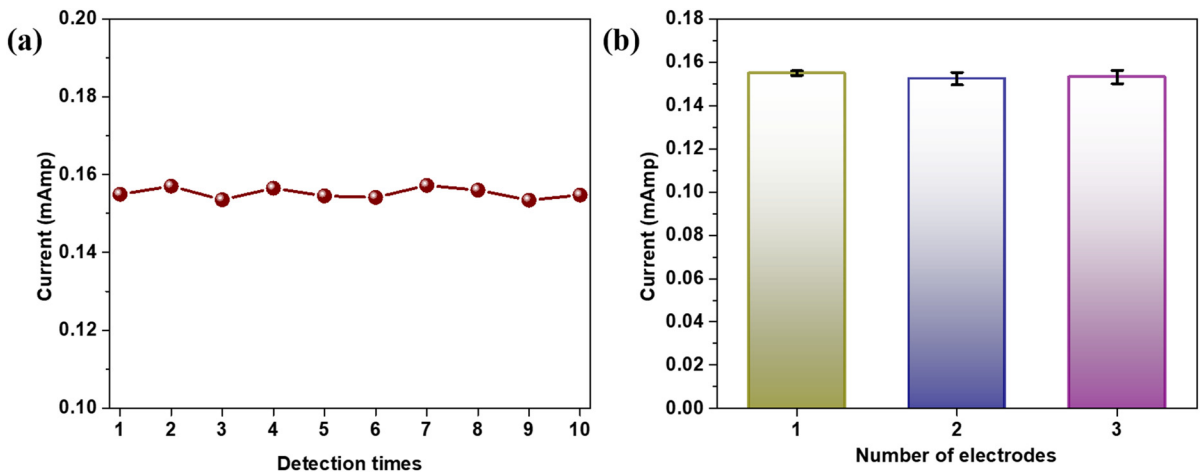


Fig. 8 Repeatability (a) and reproducibility (b) of the PPy Fls/Ni foam electrode for the detection of *p*-NP (10 nM).

 This journal is © The Royal Society of Chemistry 2024

Table 1 Comparison of electrochemical sensor performances with various modified electrode towards the detection of *p*-NP

Modified electrodes	Linear range	Correlation coefficient	Detection limit	Stability	Recovery	Ref.
Nano-gold/GCE	10–1000 μM	—	8 μM	95% (7 days)	97–97.7%	55
GO/GCE	0.1–120 μM	0.9975	0.02 μM	83% (30 days)	99.0–102.3%	56
MWNT–Nafion/GCE	0.1–10 μM	0.9980	0.04 μM	94.4% (12 h)	102.6–104.6%	57
AuNPs@cMWCNT/GCE	0.3–400 μM	0.9899	0.11 μM	88.33% (25 days)	91.2–107.9%	58
Au/$CaCO_3$/GCE	0.1–100 μM	0.9934	0.54 nM	—	94.54–96%	59
AgNWs-PANI/GCE	0.6–32 μM	0.997	52.0 nM	—	97–101.5%	60
PPy Fls/Ni foam	0.01–20 nM	0.994	7.18 pM	95% (7 days)	91–108.4%	This work

Table 2 Electrochemical analyses of *p*-NP in real water samples on the PPy Fls/Ni foam electrode

Sample	Spiked (nM)	Found (nM)	Recovery (%)
Groundwater	0	—	—
	1	0.91	91
	5	5.42	108.4
	10	9.95	99.5
Tap water	0	—	—
	1	1.05	105
	5	4.67	93.4
	10	10.04	100.4

4. Conclusion

In summary, polypyrrole (PPy) flowers were synthesized using a template-assisted method and were characterized by different techniques to investigate their morphological, structural, and chemical properties. Furthermore, the as-synthesized PPy flowers were employed as an effective electron mediator in the development of a *p*-NP chemical sensor by fabricating a PPy Fls/Ni foam electrode. The PPy Fls/Ni foam-modified electrode demonstrated a low detection limit of 7.18 pM and a dependable high sensitivity of 5.37 μA nM^{-1} cm^{-2}. The manufactured sensor's linear range was determined to be between 0.01 and 20 nM, along with a very low response time of 3.13 s. The investigation indicates that polypyrrole flowers can be effectively utilized for the fabrication of a highly sensitive and reliable *p*-NP electrochemical sensor.

Data availability

Data for this article, including SEM images of PPy flowers and raw data of Raman, FT-IR and XRD, are available at Science Data Bank at **https://doi.org/10.57760/sciencedb.09296**.

Conflicts of interest

The authors declare that they have no known competing financial interests or personal relationships that could have appeared to influence the work reported in this paper.

Acknowledgements

The authors are thankful to MRC, MNIT Jaipur, for providing characterization facilities. S. D. L. thanks MoE, Government of India, for providing the Institute Fellowship and G. P. acknowledges the support from IUAC, New Delhi (Project No.: UFR 66325), for financial support.

References

1 A. Mejri, G. Mandriota, H. Elfil, M. L. Curri, C. Ingrosso and A. Mars, *Molecules*, DOI: **10.3390/molecules27238490**.
2 M. Faisal, M. M. Alam, J. Ahmed, A. M. Asiri, M. Jalalah, R. S. Alruwais, M. M. Rahman and F. A. Harraz, *Biosensors*, 2022, **12**, 1–18.
3 Y. Zhou, J. Zhao, S. Li, M. Guo and Z. Fan, *Analyst*, 2019, **144**, 4400–4406.
4 R. Su, H. Tang and F. Xi, *Front. Chem.*, 2022, **10**, 1–11.
5 J. Liu, Y. Chen, Y. Guo, F. Yang and F. Cheng, *J. Nanomater.*, 2013, 2013.
6 Y. Tang, R. Huang, C. Liu, S. Yang, Z. Lu and S. Luo, *Anal. Methods*, 2013, **5**, 5508.
7 Y. Hu, Z. Zhang, H. Zhang, L. Luo and S. Yao, *Thin Solid Films*, 2012, **520**, 5314–5321.
8 Y. Li, Y. Ma, E. Lichtfouse, J. Song, R. Gong, J. Zhang, S. Wang and L. Xiao, *J. Hazard. Mater.*, 2022, **421**, 126718.
9 G. Li, X. Wan, Y. Xia, D. Tuo, X. Qi, T. Wang, M. Mehmandoust, N. Erk, Q. He and Q. Li, *ACS Appl. Nano Mater.*, 2023, **6**, 17040–17052.
10 X. Wan, H. Du, D. Tuo, X. Qi, T. Wang, J. Wu and G. Li, *ACS Appl. Nano Mater.*, 2023, **6**, 19403–19413.
11 U. Solaem Akond, K. Barman, A. Mahanta and S. Jasimuddin, *Electroanalysis*, 2021, **33**, 900–908.
12 M.-M. Yuan, J. Zou, J.-F. Guan, Z.-N. Huang and J.-G. Yu, *Ecotoxicol. Environ. Saf.*, 2020, **201**, 110862.
13 J. Shen, L. Liu, W. Huang and K. Wu, *Anal. Chim. Acta*, 2021, **1167**, 338594.
14 C. Li, Z. Wu, H. Yang, L. Deng and X. Chen, *Sens. Actuators, B*, 2017, **251**, 446–454.
15 Q. He, B. Wang, J. Liu, G. Li, Y. Long, G. Zhang and H. Liu, *Environ. Res.*, 2022, **214**, 114007.
16 V. Kumar, K. Singh, S. Panwar and S. K. Mehta, *Int. Nano Lett.*, 2017, **7**, 123–131.

17 T. Wang, Y. Xia, X. Wan, Y. Zhang, N. Chen, Y. Jin and G. Li, *Microchem. J.*, 2024, **201**, 110673.
18 G. Li, X. Qi, J. Wu, X. Wan, T. Wang, Y. Liu, Y. Chen and Y. Xia, *Food Chem.*, 2024, **436**, 137753.
19 M. Yu, L. Wu, J. Miao, W. Wei, A. Liu and S. Liu, *Anal. Chim. Acta*, 2019, **1080**, 84–94.
20 A. Bagheri and M. Hassani Marand, *Russ. J. Electrochem.*, 2020, **56**, 453–461.
21 S. D. Lawaniya, S. Kumar, Y. Yu, H.-G. Rubahn, Y. K. Mishra and K. Awasthi, *Mater. Today Chem.*, 2023, **29**, 101428.
22 S. M. Oliveira, J. M. Luzardo, L. A. Silva, D. C. Aguiar, C. A. Senna, R. Verdan, A. Kuznetsov, T. L. Vasconcelos, B. S. Archanjo, C. A. Achete, E. D'Elia and J. R. Araujo, *Thin Solid Films*, 2020, **699**, 137875.
23 H. Zhou, G. Xu, A. Zhu, Z. Zhao, C. Ren, L. Nie and X. Kan, *RSC Adv.*, 2012, **2**, 7803–7808.
24 S. D. Lawaniya, S. Kumar, Y. Yu, Y. K. Mishra and K. Awasthi, in *Complex and Composite Metal Oxides for Gas VOC and Humidity Sensors*, Elsevier, 2024, vol. 1, pp. 107–150.
25 A. D. Arulraj, M. Vijayan and V. S. Vasantha, *Anal. Chim. Acta*, 2015, **899**, 66–74.
26 F. Z. Tighilt, S. Belhousse, A. Rahal, K. Hamdani, N. Belhaneche, S. Sam and K. Lasmi, *Silicon*, 2022, **14**, 4149–4155.
27 M. Faisal, M. M. Alam, J. Ahmed, A. M. Asiri, M. Jalalah, R. S. Alruwais, M. M. Rahman and F. A. Harraz, *Biosensors*, 2022, **12**, 990.
28 S. D. Lawaniya, S. Kumar, Y. Yu and K. Awasthi, *Sens. Actuators, B*, 2023, **382**, 133566.
29 J.-G. Wang, B. Wei and F. Kang, *RSC Adv.*, 2014, **4**, 199–202.
30 J. G. Wang, Y. Yang, Z. H. Huang and F. Kang, *Electrochim. Acta*, 2014, **130**, 642–649.
31 H. Farrokhi, O. Khani, F. Nemati and M. Jazirehpour, *Synth. Met.*, 2016, **215**, 142–149.
32 O. Khani, F. Nemati, H. Farrokhi and M. Jazirehpour, *Synth. Met.*, 2016, **220**, 567–572.
33 J. Zhang, X. Liu, L. Zhang, B. Cao and S. Wu, *Macromol. Rapid Commun.*, 2013, **34**, 528–532.
34 X. Fan, Z. Yang and N. He, *RSC Adv.*, 2015, **5**, 15096–15102.
35 Y. Wang, A. Wang, P. Yang, W. Hu, X. Guo, J. Zhang, C. Li and C. Zhang, *J. Mater. Sci. Chem. Eng.*, 2017, **05**, 26–43.
36 M. Feng, W. Lu, Y. Zhou, R. Zhen, H. He, Y. Wang and C. Li, *Sci. Rep.*, 2020, **10**, 1–12.
37 S. Yang, C. Shen, Y. Liang, H. Tong, W. He, X. Shi, X. Zhang and H. J. Gao, *Nanoscale*, 2011, **3**, 3277–3284.
38 A. F. Diaz, J. I. Castillo, J. A. Logan and W.-Y. Lee, *J. Electroanal. Chem. Interfacial Electrochem.*, 1981, **129**, 115–132.
39 A. G. MacDiarmid and A. J. Epstein, *Faraday Discuss. Chem. Soc.*, 1989, **88**, 317.
40 J. Arjomandi, A.-H. A. Shah, S. Bilal, H. Van Hoang and R. Holze, *Spectrochim. Acta, Part A*, 2011, **78**, 1–6.
41 M. A. Chougule, S. G. Pawar, P. R. Godse, R. N. Mulik, S. Sen and V. B. Patil, *Soft Nanosci. Lett.*, 2011, **01**, 6–10.
42 V. Hernandez, F. J. Ramirez, G. Zotti and J. T. López Navarrete, *Chem. Phys. Lett.*, 1992, **191**, 419–422.
43 S. D. Lawaniya, S. Kumar, Y. Yu and K. Awasthi, *Sci. Rep.*, 2024, **14**, 7904.
44 S. D. Lawaniya, N. Meena, S. Kumar, Y. Yu and K. Awasthi, *IEEE Sens. J.*, 2022, **23**, 1–1.
45 S. Ahmad, I. Khan, A. Husain, A. Khan and A. M. Asiri, *Polymers*, 2020, **12**, 3047.
46 R. Turczyn, K. Krukiewicz, A. Katunin, J. Sroka and P. Sul, *Compos. Struct.*, 2020, **232**, 111498.
47 S. D. Lawaniya, S. Kumar, Y. Yu and K. Awasthi, *ACS Appl. Polym. Mater.*, 2023, **5**, 1945–1954.
48 Y. Sood, S. D. Lawaniya, H. Mudila, K. Awasthi and A. Kumar, *Sens. Actuators, B*, 2023, **394**, 134298.
49 J. Hu, Y. Li, G. Gao and S. Xia, *Sensors*, 2017, **17**, 2594.
50 V. V. Karambelkar, J. D. Ekhe and S. N. Paul, *J. Mater. Sci.*, 2011, **46**, 5324–5331.
51 A. Dianatdar, M. Miola, O. De Luca, P. Rudolf, F. Picchioni and R. K. Bose, *J. Mater. Chem. C*, 2022, **10**, 557–570.
52 J. Wu, Q. Wang, A. Umar, S. Sun, L. Huang, J. Wang and Y. Gao, *New J. Chem.*, 2014, **38**, 4420–4426.
53 M. Kumar, U. Krishnan, P. Devi and A. Kumar, *J. Mater. Sci.: Mater. Electron.*, 2018, **29**, 10–19.
54 S. Singh, N. Kumar, M. Kumar, Jyoti, A. Agarwal and B. Mizaikoff, *Chem. Eng. J.*, 2017, **313**, 283–292.
55 L. Chu, L. Han and X. Zhang, *J. Appl. Electrochem.*, 2011, **41**, 687–694.
56 J. Li, D. Kuang, Y. Feng, F. Zhang, Z. Xu and M. Liu, *J. Hazard. Mater.*, 2012, **201–202**, 250–259.
57 W. Huang, C. Yang and S. Zhang, *Anal. Bioanal. Chem.*, 2003, **375**, 703–707.
58 L. Wang, Q. Sun, Y. Liu and Z. Lu, *RSC Adv.*, 2016, **6**, 34692–34698.
59 Q. Ding, Z. Kang, L. Cao, M. Lin, H. Lin and D.-P. Yang, *Appl. Surf. Sci.*, 2020, **510**, 145526.
60 C. Zhang, S. Govindaraju, K. Giribabu, Y. S. Huh and K. Yun, *Sens. Actuators, B*, 2017, **252**, 616–623.

This journal is © The Royal Society of Chemistry 2024